Advances in Concrete Construction, *Vol. 10, No. 3 (2020) 221-236*
DOI: https://doi.org/10.12989/acc.2020.10.3.221

Laboratory investigations on the effects of acid attack on concrete containing portland cement partially replaced with ambient-cured alkali-activated binders

Kruthi K. Ramagiri[1a], Swaraj Patil[2b], Harsh Mundra[3c] and Arkamitra Kar*[1]

[1]Department of Civil Engineering, BITS Pilani-Hyderabad Campus, Telangana, India
[2]Department of Civil Engineering, Politecnico di Milano, Italy
[3]Walter P Moore LLC, Houston, Texas, USA

(*Received June 19, 2019, Revised August 11, 2020, Accepted August 5, 2020*)

Abstract. To reduce the CO_2 emissions associated with the manufacture of portland cement (PC), an efficient alternative like an alkali-activated binder (AAB) is the requirement of the industry. To promote the use of AAB in construction activities, a practically implementable mix proportion is required. Owing to the several raw ingredients of AAB concrete and their associated uncertainties, partial replacement of PC by AAB may be adopted instead of complete replacement as per industrial requirements. Hence, the present study aims to determine an optimal proportion for partial replacement of PC with AAB and recommend a technique for it based on site conditions. Three modes of partial replacement are followed: combining all the dry ingredients for AAB and PC followed by the addition of the requisite liquids (PAM); combining the PC and the AAB concrete in two horizontal layers (PAH); and two vertical layers (PAV). 28-day old specimens are exposed to 10% v/v solutions of HCl, H_2SO_4, and HNO_3 to evaluate changes in mechanical, physical, and microstructural characteristics through compressive strength, corrosion depth, and microscopy. Based on deterioration in strength and integrity, PAH or PAV can be adopted in absence of acid attack, whereas PAM is recommended in presence of acid attack.

Keywords: alkali-activated binder; mixing proportion; acid resistance; microstructure

1. Introduction

The decomposition of limestone for cement production has a two-fold effect on nature - (i) it emits a substantial amount of CO_2, and (ii) it reduces limestone resources. Moreover, the rapid development of infrastructure all over the world has led to a shortage of cement in various places. In the absence of any other viable alternative for portland cement (PC), this situation may lead to huge demand and a low supply of cement, thereby hindering sustainable development. These issues call for a need to develop and design an alternative material, which will reduce the demand for PC and simultaneously decrease the CO_2 emission. In order to be a suitable alternative to PC, the proposed material must also possess mechanical and structural properties comparable to PC. As a possible solution, the use of alkali-activated binders (AAB) and concrete with AAB have attracted global interest over the past two decades (Provis *et al.* 2015). AAB is produced by the reaction of aluminosilicate-rich industrial by-products like fly ash and/or slag with an alkaline solution composed of sodium silicate (Na_2SiO_3) and sodium hydroxide (NaOH).

Most of the studies to date show prolific research on the mechanical behavior of heat-cured AAB (Diaz-Loya *et al.* 2011, Provis *et al.* 2014, Shekhovtsova *et al.* 2015, Ding *et al.* 2016, Xie *et al.* 2019). Indispensable heat-curing of fly ash based AAB is attributed to its slow reaction kinetics (Ismail *et al.* 2014). Previous research on ambient-cured AAB shows that incorporation of slag was instrumental in not only improving its mechanical performance but also eliminating the otherwise requisite heat-curing (Kar *et al.* 2016, Rashad 2013, Nath and Sarker 2014, Fang *et al.* 2018, Ramagiri *et al.* 2020). This is attributed to the positive effect of Ca^{+2} ions. Addition of calcium-rich precursor results in formation of geopolymeric matrix and calcium aluminosilicate hydrate matrix (C-A-S-H) (Yip *et al.* 2005) which enhances the compressive strength of AAB. Ambient-cured AAB will be instrumental in not only reducing the energy associated with heat-curing but promoting the practical use of AAB in the field, as in-situ heat curing is impractical (Kumar *et al.* 2010). One of the significant incentives for promoting the practical use of concrete with AAB is the annual output of fly ashes from power plants. As per the report from central electricity authority, India, with data collected from over 155 thermal plants, around 169.25 MT of fly ash is produced in the year 2016-17, with 36.72 percent still unutilized (Central electricity authority 2017). This is humongous enough to demand a constant need to find new uses for them. Also, fly ash is available free of cost. For the reasons discussed previously, the usage of slag is highly recommended in ambient-cured AAB. Slag has high water demand and is nearly half as expensive as PC (Duxson 2009). This

---

*Corresponding author, Assistant Professor
E-mail: arkamitra.kar@hyderabad.bits-pilani.ac.in
[a]Ph.D. Candidate
[b]Graduate Student
[c]Graduate Engineer-Diagnostics

http://www.techno-press.org/?journal=acc&subpage=7
ISSN: 2287-5301 (Print), 2287-531X (Online)

accentuates the need to arrive at an optimum proportion of fly ash and slag depending on strength requirements and economic considerations. The main advantages of using AAB are low energy consumption and lesser cost of production (Kani *et al.* 2018, Luukkonen *et al.* 2018). The proportions of the raw ingredients govern the mechanical and serviceability characteristics of the concrete with AAB. Unlike PC, the performance of AAB depends on different ratios of its primary elements, which are most of the times interlinked increasing the complexity of control. The parameters that govern the final performance of AAB are water/solids (w/s) ratio, alkaline liquid/binder ratio, temperature and time of curing, molarity of sodium hydroxide, SiO_2/Na_2O ratio of silicate solution and activating solution (Ms modulus) and the proportioning of precursors. The authors highlight the following key points as the synthesis from existing literature:

- w/s ratio has an inverse impact on the strength of AAB;
- alkaline liquid/binder ratio governs the workability of the mix;
- increasing time and temperature of curing enhances the strength of AAB;
- strength improves by increasing silicates-to-oxides ratio, consequently increasing the unit cost of the mix;

it is recommended that for low-carbon systems (AAB), the ratio of SiO_2/Na_2O in the sodium silicate should be around 2

Hence it is of paramount importance to follow the proper order and maintain the required quantities of these raw materials during the preparation of AAB (Kar 2013, Wallah and Rangan 2006, Rangan 2008). In the present study, only the proportion of precursors is varied in AAB, maintaining other ratios, time and temperature of curing as constant. The required details of the mix are presented in section 2.2. The guidelines of the RILEM TC-224 (Provis and van Deventer 2014) are the only ones available for the practical use of AAB. Mixing procedure is known to significantly affect the fresh properties and compressive strength of AAB concrete (Hardjito and Rangan 2005, Palacios and Puertas 2011). RILEM TC-224 proposed two mixing procedures with the only difference in the order of adding the precursors (Ko *et al.* 2014). The mix procedures adopted for AAB concrete by different researchers are summarized below:

1. The activator solution was prepared at least 24 hours before the casting. Dry mixing of aggregates and the precursors for 2 minutes was followed by the addition of alkaline activating solution and superplasticizer, which was added to maintain a slump height of 75-100 mm even at water-to-solid ratios below 0.4. The mixing time was 5 minutes (Rangan 2010).
2. Precursors were mixed with hydroxide solution for the first 3 minutes, followed by the addition of silicates. The mixing was continued for another 2 minutes. Aggregates were mixed for another 2 minutes, followed by the incorporation of any additional water and superplasticizer. The mixing continued for 3 more minutes (Diaz-Loya *et al.* 2011).
3. All the dry raw materials viz. aggregate and the precursors were mixed initially for 2 minutes. The blending of the silicate solution for 2 minutes was followed by the addition of the hydroxide solution. The mix is then blended for 2 more minutes. The remaining water and superplasticizer are then mixed for 2 minutes (Junaid *et al.* 2015).

In several countries around the globe and specifically the Indian scenario, industrial demand for AAB concrete is still practically negligible. The uncertainty in composition of the fly ash and slag precursor and the potentially corrosive nature of the alkaline activator are perceived to be the main reasons for this hindrance. So, to encourage its practical usage, the authors feel that partial replacement of PC with AAB will provide a stepping stone for more widespread future applications. A recent study on fly ash-based AAB compares four different mixing techniques with varied sequence of adding the ingredients (Dassekpo *et al.* 2017). It is reported that addition of (fly ash+sand), followed by sodium hydroxide, sodium silicate, plasticizer and additional water, in the specified sequence, exhibited higher compressive strength compared to other mixing sequences. This mixing sequence is similar to the procedure proposed by Diaz-Loya *et al.* (2011). However, the study is on only fly ash-based AAB mortar and considers only the effect on the compressive strength. The workability of the mix is also of high significance if it has to be proposed for field applications. There are studies reported on the effect of mixing sequence and mixing time on the performance of AAB (Dassekpo *et al.* 2017, Palacios and Puertas 2011). The most significant work regarding concrete containing ambient-cured PC-AAB hybrid mix is the one conducted by Askarian *et al.* (2018). Ambient-cured one-part hybrid PC-AAB concrete mixes with solid potassium carbonate as activator was proposed for on-site construction of structural members. PC proportion was varied from 10% to 60% of the total binder containing PC, fly ash, and slag. The compressive strength of the hybrid mixes was observed to be higher than that of the control PC mixes. This study showed encouraging signs for the on-site preparation of hybrid PC-AAB mixes. However, no study is reported on standardizing the mixing technique for partial replacement of PC with AAB. This constitutes the rationale behind the first objective of this study as detailed later in the manuscript.

The authors believe that improved compressive strength alone cannot be used as justification for practical widespread application of AAB concrete. The performance of AAB concrete over time must supplement the enhanced strength values. Existing literature shows several studies on the superior resistance of AAB concrete to acid attack compared to its PC counterpart. However, there are no studies reported on the effect of acid attack on these hybrid mixes. So, this aspect is selected for developing the second objective of this study, which is described later in the manuscript.

AAB concrete is known to exhibit superior acid resistance in comparison to PC when tested using both accelerated and non-accelerated tests (Lee and Lee 2016, Gu *et al.* 2018, Aiken *et al.* 2018). The difference in the behavior of PC concrete and AAB concrete on the acid attack is attributed to different reaction products formed. The primary reaction product of PC, which is C-S-H, undergoes decalcification, and $Ca(OH)_2$ dissolves in acid. Alkali-activated slag (AAS) exhibits higher resistance to acid attack compared to PC owing to lower CaO content, which is approximately 40% in AAS in contrast to approximately 65% in PC. The higher resistance of alkali-activated fly ash, prominently referred to as geopolymers, in some aggressive environments in contrast to PC is attributed to a highly crosslinked aluminosilicate matrix (Lee and Lee 2016). The primary reaction product of blended AAB concrete, when fly ash and slag are used as precursors is sodium aluminosilicate hydrate [N-A-S-H] and C-(A)-S-H matrix. Both these products on acid attack form an intact layer of other reaction products, depending on the type of acid (Lloyd *et al.* 2012, Shi 2003). When both fly ash and slag are used as precursors, N-A-S-H, and C-(A)-S-H co-exist, increasing the complexity of their chemistry (Yip *et al.* 2008, Ramagiri and Kar 2019). Very few studies are reported on the resistance of blended AAB to acid attack, and further investigation on the underlying mechanisms relating the changes in the reaction products and the acid resistance potential of AAB is necessary. Existing literature on fly ash and slag blended AAB exposed to relatively concentrated sulfuric acid attack reveals that the corrosion mechanism of the hardened paste is a two-stage process (Allahverdi and Škvára 2005, Allahverdi and Škvára 2006):

- Stage 1: The charge-compensating cations from the framework (Ca^{+2} and Na^{+}) participate in ion-exchange reaction with H^{+} and H_3O^{+} from the solution. Additionally, the acid protons attack the polymeric Si-O-Al chain ejecting Al from the tetrahedral framework.
- Stage 2: The exchanged Ca ions react with diffusing sulfate ions form the acid forming protective layer of gypsum crystals which inhibits further attack.

At low concentrations of sulfuric acid ($pH \approx 3$) and for an exposure period of a minimum 90 days, the corrosion mechanism includes leaching of charge-compensating cations and Al from the tetrahedral framework. But, formation of gypsum crystals is not observed at such low concentrations of the acid (Allahverdi and Škvára 2005, Allahverdi and Škvára 2006). The extent of the sulfuric acid attack is governed by the porosity of the matrix. With increasing slag content and consequent formation of C-A-S-H matrix results in a denser matrix delaying the degradation due to acid attack. Despite its low contribution to the strength, N-A-S-H is found to be more resistant to the sulfuric acid attack compared to C-A-S-H which decalcifies to form gypsum (Lee and Lee 2016). This highlights the importance of optimizing the slag content in the AAB mix to achieve desired strength and durability performance.

The chemical degradation of concrete due to acid attack can be evaluated using different measures like mass loss, strength loss, and corrosion depth. The majority of studies reported the mass loss of AAB on immersion in acid (Song *et al.* 2005, Pacheco-Torgal *et al.* 2010, Lee and Lee 2016). Only a few reported strength loss and corrosion depth (Song *et al.* 2005, Bakharev *et al.* 2003, Lloyd *et al.* 2012, Allahverdi and Škvára 2005, Bernal *et al.* 2012, Gu *et al.* 2018). Provis and van Deventer (2014) reported that the percentage of mass loss is related to the geometry of the sample (Provis and van Deventer 2014). Estimation of degradation using mass change also requires addressing the problems associated with the regulation of pore water (Gu *et al.* 2018). Hence, mass loss is not an appropriate measure to characterize the degradation due to the acid attack in the case of AAB concrete. The present authors opine that strength loss and corrosion depth measurements are reliable in estimating the extent of the attack compared to mass change.

The authors also believe that the observations made on the strength and acid-resistance studies need to be corroborated by changes in mineralogy and microstructure of the PC-AAB hybrid binder systems. Thus, the third crucial aspect under consideration for this study is the microstructure of the hardened PC+AAB systems. Askarian *et al.* (2018) reported the formation of a combined N-A-S-H, C-A-S-H, and C-S-H matrix for the hybrid binder systems. This combined network is directly connected to the considerably higher early-age and ultimate strength of these hybrid mixes. As this study considers the effect of acid attack, the authors also review the effect of acid exposure to the microstructure of AAB and then on the PC-AAB hybrid systems. A recent study reported the significance of molecular alteration of AAB when exposed to sulfuric acid using a synthetically prepared N-C-A-S-H matrix. A higher concentration of sulfuric acid resulted in the formation of calcium monosulfoaluminate (AFm) and ettringite and/or gypsum (Zhang *et al.* 2018, Ye and Huang 2020). The formation of ettringite is governed by calcium content, and Al/Si ratio controls the formation of AFm in the acid-exposed AAB systems (Ye and Huang 2020). The Al/Si ratio is greater in uncorroded layers compared to corroded layers; however, this difference becomes negligible with increasing slag content in blended AAB (Zhang *et al.* 2018). So, the third objective of this study is developed to determine the microstructural characteristics of hybrid PC-AAB binder systems and establish a correlation between these characteristics and the mechanical properties.

Combining the three key issues highlighted above, the authors have identified the potential aspects of PC+AAB hybrid concrete mixes, which require further investigation. The objectives of this study are as follows:

I. This study is focused on determining an optimum mode of mixing the ingredients for producing concrete containing equal quantities (1:1) of PC and AAB under ambient curing conditions available in the Indian subcontinent. In the present study, three different modes of mixing are adopted: i) combining all the dry ingredients for AAB and PC and then mixing them in a combined blend with the relevant liquids (PAM), ii) combining the PC and AAB concrete in two horizontal layers (PAH), and iii) combining the PC and AAB in two vertical layers (PAV). The AAB compositions in these layers are also varied to evaluate the influence of slag addition to the AAB precursor. The three AAB mix proportions used in this study are 100% fly ash (FS 0), 70% fly ash + 30% slag (FS 30), and 50% fly ash + 50% slag (FS 50).

II. The next objective of this study is to determine the resistance of the proposed mixes to acid attack through changes in their physical and mechanical characteristics. The response to acid attack for PC+AAB mixes is

Table 1 Properties of the raw materials

Materials	Slag*	Fly ash
Specific gravity	2.88	2.47
Specific surface(m^2/kg)	580 (Blaine)	490 (Blaine)
Loss on ignition %	0.06	3.00
SiO_2, %	36.0	49.34
Al_2O_3, %	12.0	22.73
CaO, %	42.0	3.09
MgO, %	6.0	1.06
SO_3, %	0.2	0.97
$Na_2O + 0.685\ K_2O$, %	0.74	2.75
Fe_2O_3, %	1.8	16.01
Others, %	1.2	1.05
Percentage finer than 45μm, %	96.79	85.74
Activity index (PAI) at 28 days, as per ASTM C311/C311M-18 (ASTM C311/C311M 2018)	95[a]	85[b]

* The pH value (in water) for the slag is in the range of 10.5 ~ 12.7; [a] Slag activity index corresponding to Grade 100 as per ASTM C989; [b] Strength activity index corresponding to Class F as per ASTM C618.

compared with those of 100% PC (i.e., no replacement) mixes through testing of compressive strength and corrosion depth measurements, instead of mass loss as explained earlier. These results are aided by visual comparison using stereomicroscopic imaging.

III. The last objective of this study is to conduct a mineralogical and microstructural analysis of PC+AAB pastes through X-ray diffraction (XRD), Fourier transform infrared spectroscopy (FTIR) and scanning electron microscopy coupled with energy dispersive spectroscopy (SEM-EDS) techniques. Microstructural studies are performed before and after immersion in acid solutions to provide a clear understanding of the degradation mechanism.

Based on the observations from the present study, recommendations are made for the mixing technique to be adopted in the field during partial replacement of PC by AAB under ambient conditions available in climates similar to those of the Indian subcontinent. The following section describes the materials and experimental methods for this study.

2. Materials and mixing technique

2.1 Materials

The following materials were used in this study for the AAB mixes:

- **Fly ash**: Class F fly ash conforming to ASTM C618 (Standard Specification for Coal Fly Ash and Raw or Calcined Natural Pozzolan for Use in Concrete) (ASTM C618 2013) obtained from a local coal power plant. The specific gravity, specific surface area, and oxide composition are listed in Table 1.
- **Slag**: Ground granulated blast furnace slag or slag conforming to Grade 100 of ASTM C989 (Standard Specification for Slag Cement for Use in Concrete and Mortars) (ASTM C989 2013) obtained from the local steel plant.

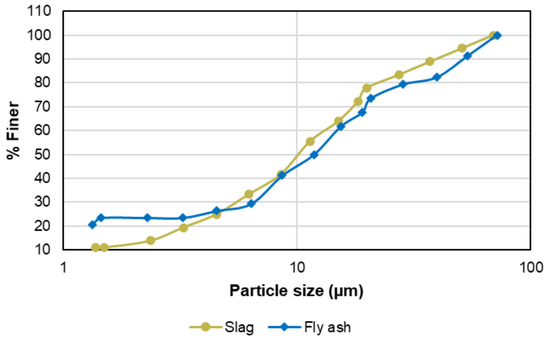

Fig. 1 Particle size distribution of precursors

- **Alkali-activators**: The sodium hydroxide pellets and sodium silicate solution are obtained from HYCHEM chemicals. The purity of sodium hydroxide pellets is 99% and conforms to food grade. The sodium silicate solution is composed of 55.9% water, 29.4% SiO_2, and 14.7% Na_2O.
- **Coarse aggregate**: 12.5 mm (½ in.) graded and crushed limestone conforming to ASTM C33/C33M - 13 (Standard Specification for Concrete Aggregates) (ASTM C33/C33M 2017). The saturated surface dry (SSD) bulk specific gravity was 2.68.
- **Sand**: Locally available 4.75 mm (0.187 in.) graded river sand conforming to ASTM C33/C33M. The fineness modulus and the SSD bulk specific gravity of sand were 2.79 and 2.59, respectively.
- **Admixture**: Commercially available high-range water-reducing admixture (HRWRA), conforming to ASTM C494 (ASTM C494 2013) Type F (Specification for Chemical Admixtures for Concrete).

The following materials were used in this study for the PC mixes:

- **Cement**: Commercially available Type I Portland Cement conforming to ASTM C33/C33M.

The particle size distribution of slag and fly ash is presented in Fig. 1 and corroborates with the findings of Mazhar and GuhaRay (2020).

2.2 Mix proportions

The mix proportions for PC are adopted from ACI 211.1-91 (Standard Practice for Selecting Proportions for Normal, Heavyweight and Mass Concrete) (ACI 211 2009) to achieve an average 28-day compressive strength of 30 MPa. The mix proportions for the concrete with AAB are selected to design a suitable mix proportion for concrete with AAB in order to achieve comparable compressive strength with that of PC. Different combinations of fly ash with slag replacement, at different ages (7 days, 28 days), and ambient curing temperatures are used for trials. For this study, ambient conditions are 31°C±2°C average temperature and 70% average relative humidity prevalent in Hyderabad, India, during the tenure of this study. The curing temperature, slag content, and water-to-solids (w/s)

Table 2 Mixture proportions

Mixture	PC (kg/m^3)	Fly ash (kg/m^3)	Slag (kg/m^3)	NaOH (kg/m^3)	Na_2SiO_3 (kg/m^3)	Sand (kg/m^3)	CA* (kg/m^3)	Water (kg/m^3)
100% PC	385	0	0	0	0	679.6	1225.0	162
50% PC + 50% FS 0	192.5	200	0	5.285	64.715	325.5	604.5	33.82
50% PC + 50% FS 30	192.5	140	60	5.285	64.715	325.5	604.5	33.82
50% PC + 50% FS 50	192.5	100	100	5.285	64.715	325.5	604.5	33.82

*CA: Coarse aggregate

ratio govern the compressive strength. The target strength for AAB concrete is fixed at M30 at 28-days age to maintain parity with PC concrete, and the combinations of the governing factors are chosen accordingly. The starting materials can be categorized into two groups-the aluminosilicate precursor and the activating solution. As the precursors are primarily composed of industrial by-products, they will lead to a lot of uncertainties in the characteristics of the finished product. Moreover, the activating solution reacts with the precursor through a polymerization mechanism, whose chemistry is yet to be fully decoded. This polymerization process governs the development of the strength of the building material, and it is dependent on several factors - (i) the ratio of SiO_2/Na_2O in the activating silicate solution (2:1 in this case), (ii) the ratio of SiO_2/Na_2O in the precursor-activating solution mixture (also known as Ms ratio or Ms modulus), (iii) the ratio of SiO_2/Al_2O_3 in the precursor (2:1 in this case), (iv) the ratio of water-to-AAB solids (w/s) (0.30, 0.35, and 0.4 are tried for preliminary strength tests), and (v) the curing temperature, i.e., the temperature at which the polymerization is allowed to occur. In this case, the curing temperature is maintained at an average of 31°C±2°C and 70% RH. For initial assessment to estimate the best Ms modulus, the compressive strength of 100 mm cube specimens is measured for different AAB mixtures, as shown in Table 2. It is observed that a combination of Ms modulus of 1.4, fly ash: slag ratio of 70:30, and w/s ratio of 0.3 resulted in the closest 28-day average compressive strength to PC concrete for AAB concrete under the aforementioned temperature and RH. The mixture proportions summarized in Table 2 are valid for the aforementioned temperature and humidity.

Changes in temperature are directly proportional to changes in compressive strength. Higher temperatures can be attained using a furnace, but the authors recommend avoiding such practice due to the associated consumption of energy. The PC mixes are prepared with water to cement (w/cm) ratio of 0.42 for full hydration. The cement content is kept at 385 kg per m^3 of PC concrete. Hence, one m^3 of 50% PC and 50% AAB will contain 0.5×385=192.5 kg of PC. Similarly, one m^3 of AAB concrete contains 400 kg of fly ash+slag. So, in this case, one m^3 of 50%PC+50% AAB concrete will contain .5×400=200 kg of fly ash+slag.

For the AAB mixes, the fine and coarse aggregate contents are kept constant at 651 kg/m^3 and 1209 kg/m^3, respectively. All the AAB mix proportions are based on the findings of Rangan (2010). These were validated in the laboratory, and the detailed calculations are presented in Kar (2013). The reason for this proportion is to obtain an average unit weight of AAB concrete between 2200 and 2600 kg/m^3 to resemble the average unit weight of 2400 kg/m^3 for PC concrete. For the PC mixes, the corresponding values are 680 kg/m^3 and 1225 kg/m^3 to obtain the aforementioned unit weight. As the w/cm ratio is taken as 0.42, no HRWRA is used for the PC mix. For the AAB concrete mixes, the HRWRA dosage varies between 0 ~ 4000 ml/m^3, 0-3200 ml/m^3, 0-2500 ml/m^3 for w/s of 0.3, 0.35, 0.4 respectively. As w/s of 0.4 or lower renders the mix very stiff and leaves significant amount of unreacted binder residue, polycarboxylate ether based HRWRA is used to facilitate the transport of water through the early-age reaction products and uniform reactions between the activator and the binders. The HRWRA dosages are selected to maintain a slump height between 75 and 100 mm to achieve medium workability of the concrete mixes. The mixing regimes are discussed in detail in the following section.

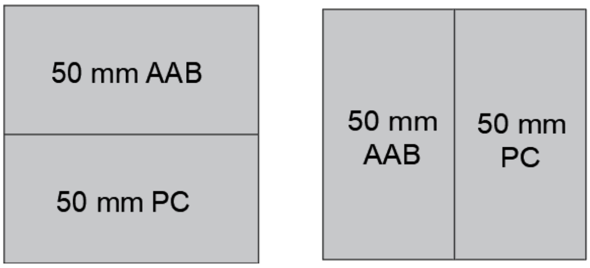

(a) Horizontal layers (b) Vertical layers

Fig. 2 Mixing of 50%PC and 50%AAB concrete in two layers

2.3 Mixing technique

The present study demonstrates the implantation of 3 types of mixing techniques described below to prepare concrete mixes containing 50% PC concrete and 50% AAB concrete.

- **Mixing of 50%PC and 50%AAB concrete in two horizontal layers (PAH)**

The 100 mm cubes consist of two horizontal layers of dimensions 100×100×50 mm each (schematically shown in Fig. 2(a)). The bottom 50 mm thick layer is composed of PC, sand, coarse aggregates, and water. The top 50 mm layer is composed of AAB containing fly ash and slag as precursors, sand, coarse aggregates, the activator solution made up of sodium hydroxide, sodium silicate, and water. The top layer is cast about 30 minutes after the bottom layer to allow for its initial setting.

- **Mixing of 50%PC and 50%AAB concrete in two**

adjacent vertical layers (PAV)

The 100 mm cubes consist of two vertical layers of dimensions 100×50×100 mm each (schematic in Fig. 2(b)). When the first layer is cast, a wooden block is placed in the other half of the cube. The ingredients are identical to those mentioned in the above mixing technique.

- **Mixing of 50%PC and 50%AAB concrete through a combination of all ingredients (PAM)**

In this type of mixing technique, PC, fly ash, and slag are first mixed with the requisite sand and coarse aggregates. The liquid solution containing sodium silicate, sodium hydroxide, and the necessary total amount of mixing water is then blended uniformly with the aforementioned dry mix.

For each of the first two mixing regimes, the dry raw materials for AAB are blended in the beginning to obtain a uniform blend. This dry blend is reacted with a liquid blend containing sodium silicate, sodium hydroxide and water according to the requirements of strength and workability. The liquid blend is prepared and stored for 24 hours prior to reacting with the dry blend to alleviate the heat evolved due to the reaction between sodium hydroxide and sodium silicate. For the final mixing regime, all the raw ingredients for PC and AAB concrete are blended uniformly, and all the liquid ingredients are blended separately before mixing these two blends uniformly to obtain the final concrete mix.

As the AAB tends to set very rapidly, the quantity of materials for three 100 mm cubes of concrete is batched at a time. For this reason, hand mixing is preferred over mixing in a mechanical mixer. The liquid and solid mixtures are combined very carefully to avoid any kind of chemical burn due to the potentially corrosive nature of the sodium hydroxide, although food-grade lye is used. The mix is prepared rapidly to ensure desirable workability while casting them into moulds. Once the concrete is poured into the moulds, the specimens are demoulded on the second day after casting. Then they are cured in water under aforementioned ambient conditions for the next 6 days. For the subsequent 21 days, the specimens are stored under ambient conditions in the laboratory until the commencement of testing. Section 4.2.4 presents the recommendations for mixing technique based on the results from the experiments described below.

3. Experimental methods

3.1 Immersion in acid solutions

After 28 days of ambient curing, three specimens each of the above kinds of PC+AAB concrete are immersed in separate 10% v/v solutions of hydrochloric, sulfuric, and nitric acids for a further 28 days, i.e., from 29th to 56th day. Additionally, three specimens for each type of concrete is stored and observed under ambient conditions for these 28 days. Hence, the compressive strength and corrosion depths are determined at the 56-day age for the specimens.

For microstructural studies, PC+AAB paste specimens (PAM mixing technique) are cast and are immersed in acid solutions on the 56th day following the similar manner explained above.

3.2 Microstructural analysis

The samples for microstructural studies are dried in an oven at a temperature of 105°C until a constant mass is reached. XRD and FTIR analysis are performed on triplicate powdered samples, whereas SEM-EDS analysis is performed on a small sample without disturbing their structure.

3.2.1 X-ray diffraction

XRD patterns were recorded on a RIGAKU Ultima X-ray Diffractometer with 2θ varying between 5-90°and the Cu Kα radiation (40 kV and 30 mA). The step size was maintained at 0.02° with a scan speed of 1°/min.

3.2.2 Fourier transform infrared spectroscopy

FTIR spectra were obtained using JASCO FT/IR-4200 over a wavenumber range of 4000-400 cm^{-1}. The sample was prepared using the KBr pellet technique. The spectra were recorded with a resolution of 4 cm^{-1} and 64 scans per spectrum.

3.2.3 Scanning electron microscopy-energy dispersive spectroscopy

For SEM-EDS analysis, FEI Apreo SEM equipped with a secondary electron and EDS detector was used. Samples were sputtered with a 10 nm layer of gold-palladium using LEICA EM ACE200 sputter coater. The micrographs were recorded at a magnification of 2500×with an operating voltage of 20 kV, and the working distance maintained constant at 10 mm. EDS analysis was performed simultaneously for each recorded micrograph.

3.3 Specimen-level testing

3.3.1 Stereomicroscopic imaging and visual inspection

Stereomicroscopic imaging is carried out to identify the particle size distribution and superficial physical features of the PC+AAB specimens using an Olympus SXZ7 setup. It is used to investigate the dimensions of the different components of the PC+AAB concrete specimens and to evaluate their changes due to acid attack. The images are captured at the magnification of 3.2×. The minimum dimension that can be identified by this microscope is 20 μm. For the sake of brevity, the stereomicroscopic images for only PAM mixes are presented in this paper.

3.3.2 Compressive strength test

The compressive strength of the cubes is determined in accordance with IS 516: 1959 (2018) (Indian Standard Method of Tests for Strength of Concrete). This code of practice is equivalent to the ASTM C39/C39M (Standard Test Method for Compressive Strength of Cylindrical Concrete Specimens) (ASTM C39/C39M 2013). Tests are conducted on the 56th day after casting, and the cube test results are presented in Table 8. The mean values of compressive strength tests for three specimens corresponding to each mix proportion along with the respective coefficients of variation (COV) are presented in Table 8.

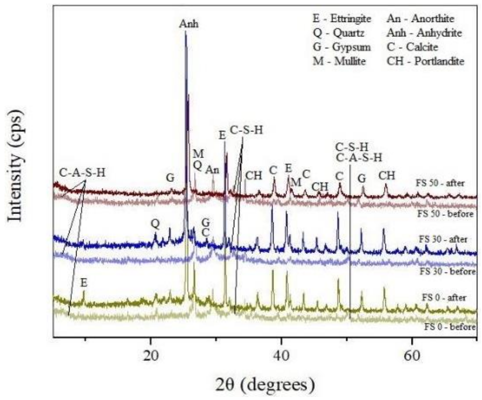

(a) Samples immersed in H_2SO_4

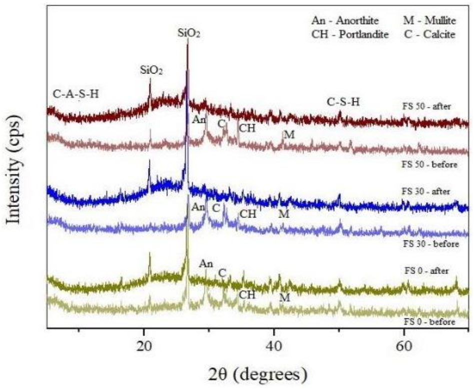

(b) Samples immersed in HNO_3

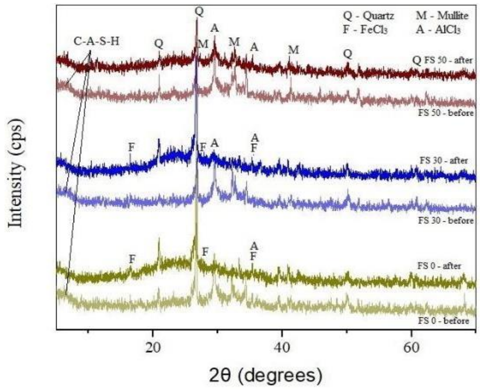

(c) Samples immersed in HCl

Fig. 3 XRD pattern of PC+AAB paste before and after immersion in acid solution

3.3.2 Test for corrosion depth

The determination of corrosion depth follows the procedure suggested in the existing literature (Zhao *et al.* 2011). Corrosion depth is defined as half of the difference between the initial width before exposure to the acid solution and the final width after brushing the corroded layer. The results obtained as mean of triplicate specimens for each mix proportion are provided in Table 9.

4. Results

4.1 Microstructural analysis

4.1.1 X-ray diffraction

Fig. 3(a) presents the X-ray diffractograms of PC+AAB paste immersed in sulfuric acid for 28 days. Unexposed PC+AAB mixes exhibit peaks of quartz, mullite, and anorthite resulted from alkaline activation of fly ash and slag, whereas peaks of C-S-H are observed due to hydration of PC. Dissolution of specimens in sulfuric acid altered the reaction products significantly, which is evident by the formation of a large number of new peaks. With an increase in the proportion of slag, the XRD pattern of both unexposed samples and those immersed in the sulfuric acid show an increase in the proportion of broad humps and a decrease in the number of peaks. This is attributed to a substantial amount of amorphous reaction products (C-S-H and C-(A)-S-H) formed on alkali-activation of PC and slag. The reaction of sulfuric acid with hydration products of PC viz. $Ca(OH)_2$, AFm, and calcium aluminate hydrates result in the formation of gypsum and ettringite. The corresponding equations are given below (Monteny *et al.* 2000).

$$Ca(OH)_2 + H_2SO_4 \rightarrow CaSO_4.2H_2O \text{ (gypsum)} \qquad (1)$$

$$\begin{gathered}3CaSO_4 + 3CaO.Al_2O_3.6H_2O + 25H_2O \rightarrow \\ 3CaO.Al_2O_3.3CaSO_4.31H_2O \text{ (ettringite)}\end{gathered} \qquad (2)$$

Upon exposure to acidic solutions, the hydrogen ions present in the acid attack anorthite framework resulting in the release of calcium and aluminum leaving tetrahedral silica. The equation representing the same is given below (Oelkers *et al.* 1995).

$$Ca_2Al_2SiO_8 + 8H^+ \leftrightarrow Ca^{2+} + 2Al^{3+} + 2SiO_2 + 4H_2O \qquad (3)$$

The absence of anorthite peaks on immersion in sulfuric acid validates its dissolution, and the released Ca ions react with sulfate ions from the acid-forming new crystalline phase of gypsum. The remaining tetrahedra of silica could result in the further formation of N-A-S-H and C-(A)-S-H gel. N-A-S-H matrix neutralizes the acid, averting further deterioration. Peaks of anhydrite observed from the diffractogram correspond to the reaction between sulfuric acid and calcium-based hydration products of the PC-AAB blended mix. The coexistence of free calcium in the AAB mix is corroborated by the formation of calcite. The peak intensity of both anhydrite and calcite increased with increasing Ca (slag) content from 0 to 30%, i.e., PC+FS 0 to PC+FS 30. Fewer peaks in the XRD pattern of PC + FS 50 immersed in sulfuric acid solution signify its greater resistance to the acid attack. This can be attributed to greater slag content and the resulting pore refinement.

XRD diffractograms of PC + AAB mixes before and after immersion in nitric acid are presented in Fig. 3b. Since the discussion on unexposed mixes is given above, and this section presents details of samples after acid attack test. The crystalline phases viz. quartz, anorthite, portlandite, and mullite dissolved in the acid, as corroborated by the absence of corresponding peaks. Immersion of samples in acid resulted in the dissolution of most of the Ca from the reaction products of PC. However, the remaining Si is converted to SiO_2. nH_2O gel, which forms a protective layer preventing further corrosion. C-(A)-S-H also decalcifies, as indicated by the reduction in the intensity of its peak in the X-ray diffractogram; the remainder aluminosilicate gel

Table 3 Characteristic IR transmission peaks of functional groups of unexposed PC+AAB mixes

Wavenumber (cm^{-1})			Assignment
PC+FS 0	PC+FS 30	PC+FS 50	
3490.5	3488.6	3497.3	ν_3 OH
3138.6	3138.6	3138.6	ν_1 OH
1640.2	1640.2	1641.1	ν_4 OH
1400.1	1401	1400.1	ν_3 CO (CO_3^{2-})
972	969.1	972	ν_3 Si-O-T (T=Si/Al)
616.2	613.3	613.3	ν_1 Si-O-T (T=Si/Al)
459.9	456.1	492.7	ν_4 Si-O and Al-O

prevents the further acid attack. Though decalcification results in a porous layer, the protective silicate and aluminosilicates layer formed is dense (Shi and Stegmann 2000, Pavlik 1994). Leaching of Ca-rich reaction products releasing Ca ions promotes the reaction of these Ca ions with NO_3^- forming soluble $Ca(NO_3)_2$ salt. However, owing to the significant amorphous nature of this salt (Gomez *et al.* 2013), it is not possible to establish its presence through XRD analysis. Therefore, FTIR analysis is performed to further characterize the degradation mechanism of PC+AAB mixes immersed in acid solutions.

Fig. 3(c) plots the XRD patterns of PC+AAB paste before and after immersion in 10% v/v hydrochloric acid solution. The extent of degradation is low in comparison to sulfuric and nitric acid attack. However, similar to the other acid attacks, leaching of Ca-bearing reaction products is evident with the formation of new phases of $AlCl_3$ and $FeCl_3$ (De Ceukelaire 1992). The intensity of peaks corresponding to anorthite and mullite decreases after immersion, which is related to the dissolution of these phases. Attack by the protons (H+) of the acid on these phases releases Al ions, which further reacts with remaining chloride ions of the acid. The peaks corresponding to $FeCl_3$ are observed only in fly ash-rich mixes viz. PC+FS 0 and PC+FS 30 owing to the higher proportion of Fe in these mixes (Temuujin *et al.* 2011).

Owing to the limitation in identifying amorphous reaction products, XRD analysis alone cannot provide a complete characterization of the reaction products formed on the acid dissolution of PC+AAB mixes. Therefore, FTIR analysis is also performed to further understand the mechanism of deterioration.

4.1.2 Fourier transform infrared spectroscopy

Fig. 4 presents the comparison of the FTIR spectra of PC+AAB mixes before and after immersion in acid solutions. For an exposure condition (immersion in acid), the FTIR spectra of three mixes: PC+FS 0, PC+FS 30, and PC+FS 50 show similar variation in the spectra with a shift in the position of bands depending on the slag content.

For PC+FS 0, the major bands observed at 3490 and 3139 cm^{-1} corresponds to asymmetric stretching of the O-H bond of absorbed water. The peak at 2869 cm^{-1} is due to the presence of calcite confirms the reaction of PC. The strong band at 1640 cm^{-1} is ascribed to deformation vibrations of H-O-H of water molecules associated with the system. The samples are stored under ambient conditions of the laboratory; hence, mild carbonation experienced is evident from transmission peaks at 1400 cm^{-1} associated with CO_3^{2-}.

Table 4 Characteristic IR transmission peaks of functional groups of PC+AAB mixes after sulfuric acid attack test

Wavenumber (cm^{-1})			Assignment
PC+FS 0	PC+FS 30	PC+FS 50	
3427.9	3433.6	3423	ν_3 OH
-	-	2134.8	ν O-S-O
1637.3	1638.2	1638.2	ν_1 OH
1285.3	1285.3	-	Bending CO
1165.8	1157.1	-	ν_3 Si-O-Si
-	1105	1105.2	ν_3 SO_4^{2-}
1010.5	-	-	ν_3 Si-O-Si
885.2	885.2	885.2	ν Si-OH
851.4	851.4	852.4	ν T-OH (T=Al/Si)
674	674	675	ν_4 SO_4^{2-}
614.2	615.2	615.2	ν_1 Si-O-T (T=Si/Al)
589	591.1	593	ν_4 SO_4^{2-}
456.1	456.1	459	ν_4 Si-O and Al-O

Bands at 972 cm^{-1} and 616 cm^{-1} ascribed to asymmetrical and symmetrical stretching of Si-O-Si (Al) bonds, respectively, substantiate alkaline activation of fly ash resulting in the formation of polymeric silicate and aluminate chains. The peak at 460 cm^{-1} evinces in-plane bending of Al-O and Si-O linkages of the aluminosilicate structure. The shift in the position of peaks for PC+FS 30 and PC+FS 50 mixes elucidates the structural changes in the aluminosilicate matrix formed. These shifts are significantly influenced by the concentrations of silicate monomer present in the activating position of Si-O-Si or Si-O-Al units (Madavarapu 2014). The main peaks and the associated vibrations for all three mixes are presented in Table 3. Dissolution of samples in sulfuric acid significantly altered the PC+AAB mixes (Fig. 4(a)) The variations in the spectral patterns of PC+AAB mixes are conspicuous on immersion in acid solutions. These variations in contrast to unexposed PC+AAB mixes are more prominent on immersion in sulfuric acid, validating its severe deterioration. Decalcification of C-(A)-S-H and formation of gypsum in FS 50, identified by the band at 2135 cm^{-1}, is ascribed to greater Ca content due to slag. The new band at 1285 cm^{-1} is attributed to C-O bending vibrations, which is noticed in spectra of FS 0, decreases its intensity in FS 30, and evanesce in FS 50. The presence of this band indicates probable carbonation in the sample, owing to a more porous matrix as a result of weak resistance of the N-A-S-H matrix to sulfuric acid attack. The band at 1166 cm^{-1} is assigned to quartz as it is the crystalline phase observed in both PC and AAB concrete. As already mentioned, greater amounts of Ca in the system results in the formation of gypsum as identified by the band at 1105 cm^{-1} in FS 30 and FS 50, attributed to asymmetric stretching of SO_4^{2-}. The minor peaks at 885 and 851 cm^{-1} are assigned to stretching of Si-OH and T-OH (T=Si/Al), respectively, and they correspond to dissolved silicate and/or aluminosilicate species. The appearance of new bands at 674 cm^{-1} and 589 cm^{-1}

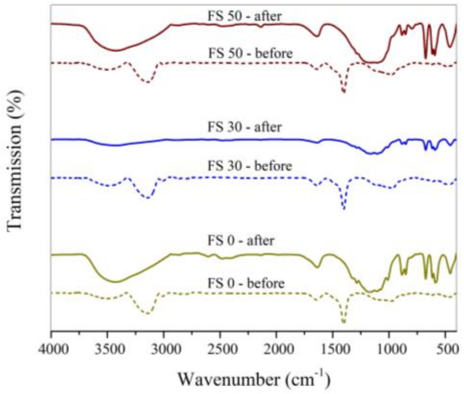

(a) Samples immersed in H_2SO_4

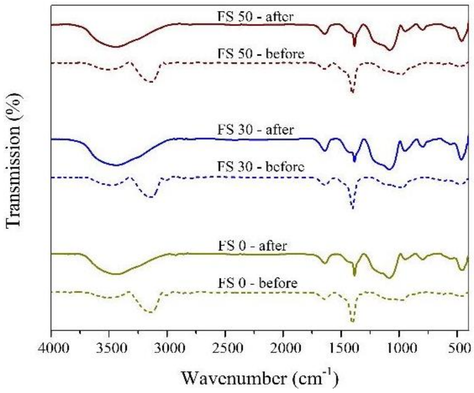

(b) Samples immersed in HNO_3

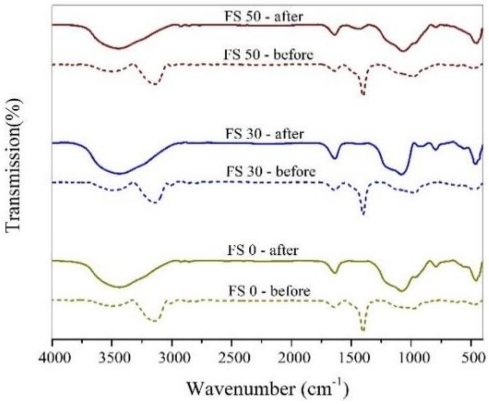

(c) Samples immersed in HCl

Fig. 4 FTIR Spectra of PC+AAB paste before and after immersion in acid solution

associated with asymmetric bending of SO_4^{2-} units of gypsum formed on the acid attack. The prominent peaks observed in the spectra of PC+AAB paste after immersion in sulfuric acid and their respective assignments are presented in Table 4.

Similar to sulfuric acid, nitric acid and hydrochloric acid decalcify the matrix phase rich in Ca. The leaching process includes the replacement of Na and Ca ions from the aluminosilicate framework by the protons from acid. These acid protons also electrophilically attack the polymeric Si-O-T (T=Al/Si) chains, resulting in the expulsion of tetrahedrally coordinated Al from the aluminosilicate framework. This results in the silicate-rich polymeric chain, and the expelled Al converts to an octahedrally coordinated Al and recombines, resulting in an intra-aluminosilicate framework (Allahverdi and Škvára 2005). This explains the reason for the shift in the position of bands corresponding to similar vibrations for samples immersed in different acid solutions. The bands additionally formed on the nitric acid attack are observed at 1384 and 945 cm^{-1} (Fig. 4(b)). The band at 1384 cm^{-1} is assigned to stretching vibration of the nitrate group, possibly corresponds to the soluble Ca-salt of nitric acid ($Ca(NO_3)_2.H_2O$) formed on decalcification. The band at 945 cm^{-1}, ascribes polymerization of the silicate group. A similar band at 964 cm^{-1} is observed in PC+FS 0 mix immersed in HCl (Fig. 4(c)), attributed to stretching of Si-O. PC is more vulnerable to acid attack, due to the dissolution of the C-S-H phase, but not fly ash and slag. Therefore, the band observed at 964 cm^{-1} concurs with the spectrum of the C-S-H matrix. The remnant peaks are associated with the same bonds as discussed for sulfuric and nitric acid attack, with a shift in the position of the peak. The characteristic vibrations and the position of peaks for PC+AAB immersed in nitric acid and hydrochloric acid are given in Table 5 and Table 6.

4.1.1 Scanning electron microscopy-energy dispersive spectroscopy

Fig. 5 presents the SEM micrographs of unexposed PC+AAB mixes. No significant variations in the micrographs are attributed to the presence of PC. However, a higher proportion of unreacted fly ash spheres are noticed in the PC+FS 0 mix. With increasing slag content, FS 50 mix exhibited relatively uniform surface morphology.

On exposure to sulfuric acid, the change in the morphology is evident from the micrographs presented in Fig. 6. As identified from XRD and FTIR studies, the formation of gypsum and ettringite is clearly visible. The proportion of these products increased with increasing slag content due to higher calcium content. Gypsum formation is evident from the micrograph captured at a magnification of

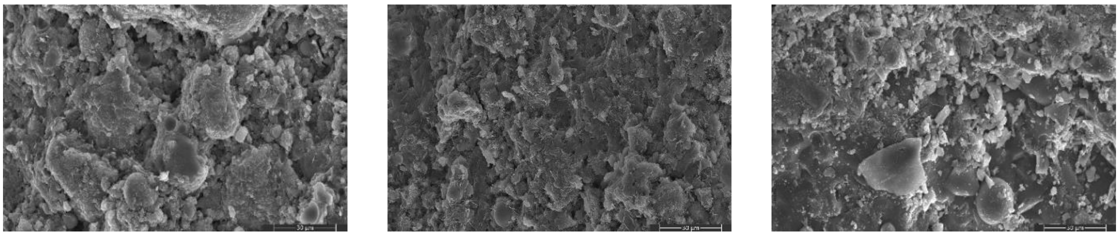

(a) PC + FS 0 (b) PC + FS 30 (c) PC + FS 50

Fig. 5 SEM micrographs of unexposed PC+AAB mixes

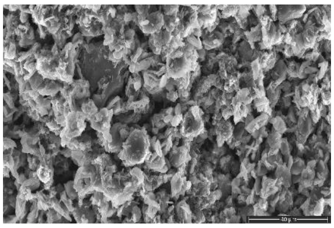

(a) PC + FS0 at 2500x

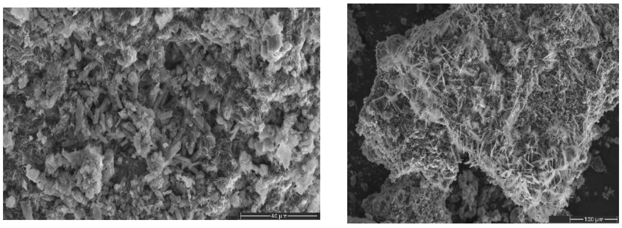

(b) PC + FS30 at 2500x (c) PC + FS30 at 600x

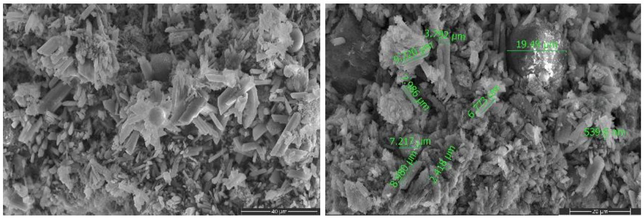

(d) PC + FS50 at 2500x (e) PC + FS50 at 2500x

Fig. 6 SEM micrographs of PC + AAB paste after H_2SO_4 attack

5000x (Fig 6(e)). The size of these crystals varied from approximately 2-10µm. The high degree of deterioration of immersion in sulfuric acid is evident from significantly higher precipitates observed from the micrographs.

SEM micrographs of PC+AAB mixes exposed to nitric, and hydrochloric acid are presented in Fig. 7.

The changes in the morphology of these samples are not as severe as the sulfuric acid attack, indicated by a lower extent of precipitation. However, PC+FS 0 mix exhibited significant deterioration of all the mixes. This is attributed to a more porous matrix result in easy ingress of acid solutions promoting the dissolution of reaction products. This increased depth of acid ingress into samples is substantiated by visual inspection results.

Table 7 Atomic percentages of elements from EDS analysis

Exposure condition	Mix	Na (%)	Al (%)	Si (%)	Ca (%)	Fe (%)
unexposed	FS 0	1.66	2.29	11.56	6.87	0.78
	FS 30	2.27	2.66	7.59	9.94	0.62
	FS 50	1.84	1.9	8.23	10.47	0.60
H_2SO_4	FS 0	0.39	1.30	7.50	6.08	0.26
	FS 30	0.64	0.82	1.97	8.77	0.54
	FS 50	0.22	0.25	3.06	9.76	0.11
HNO_3	FS 0	0.16	3.27	19.22	1.29	0.39
	FS 30	0.53	1.53	15.63	1.41	0.15
	FS 50	0.19	3.48	14.69	0.99	2.02
HCl	FS 0	0.23	1.8	13.98	1.69	2.33
	FS 30	0.17	3.36	16.64	0.72	0.36
	FS 50	0.18	4.87	19.41	1.67	1.17

Table 7 presents the average atomic percentages of the primary elements observed in the reaction products. The variation in Na, Ca, and Fe contents on exposure to acid solutions are attributed to leaching of the reaction products (Table 7). In the unexposed samples, higher Ca content in FS 50 is due to more slag. Similarly, with an increase in fly ash proportion, Fe content is increased. The greater reaction of fly ash in the presence of slag is validated by higher Na and Al percentage in PC+FS 30 mix.

It is evident from Table 7 that immersion of samples in the acid solutions leached and morphed the reaction products. Samples dissolved in sulfuric acid show a decrease in Na, Al, Si, and Fe contents. However, similar Ca content is attributed to precipitation of various Ca-bearing phases like gypsum, ettringite, and CH. It is well known that sulfuric acid is the strongest acid and, therefore, easily loses a proton. This promotes the reaction between released SO_4^{2-} ions and the leached Ca.

Low Ca content in samples immersed in nitric and

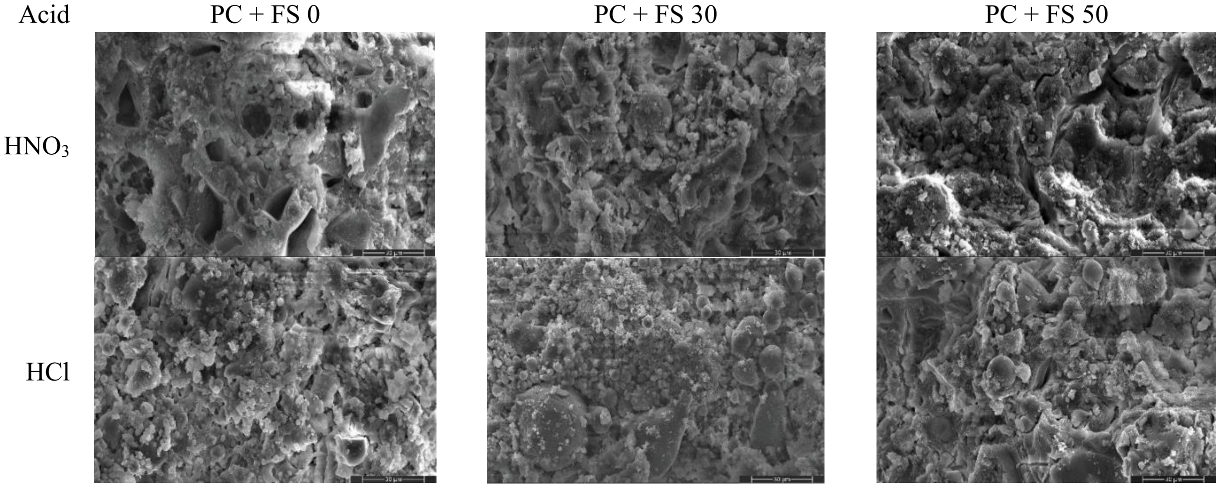

(a) PC + FS 0 (b) PC + FS 30 (c) PC + FS 50

Fig. 7 SEM micrographs of PC + AAB paste after HNO_3 and HCl attack

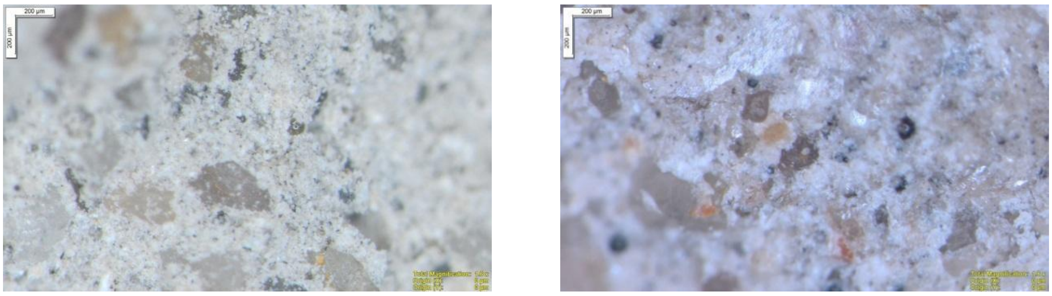

(a) air (b) 10% v/v H_2SO_4 for 28 days

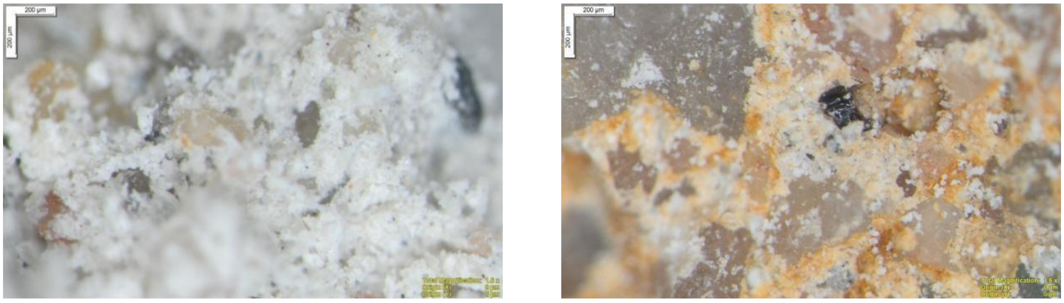

(c) 10% v/v HCl for 28 days (d) 10% v/v HNO_3 for 28 days

Fig. 8 Stereomicroscopy images for 56-day old PAM mixes at 3.2×

hydrochloric acid is due to the absence of such Ca-rich precipitates. But, equivalent Al and Si contents of these samples, relative to unexposed samples, indicate higher resistance to acid attack. This might be attributed to long-chain polymer reaction products, N-A-S-H and C-(A)-S-H.

These changes in the microstructure govern the specimen-level properties of the concrete. Hence, the following section discusses the results of specimen-level testing of PC+AAB mixes.

4.2 Specimen-level testing

4.2.1 Stereomicroscopic imaging and visual inspection

Fig. 8(a) presents the stereomicroscopic image for 56-day old PAM specimens without immersion in acid, and 56-day specimens with 28-day immersion in separate 10% v/v solutions of sulfuric acid (Fig. 8(b)), hydrochloric acid (Fig. 8(c)), and nitric acid (Fig. 8(d)), at 3.2x magnification. Visual comparison of PAM specimens after and before exposure to the acids shows whitish deposition on the surface in the case of sulfuric acid (Fig. 8(b)). HCl immersion leads to the formation of whitish to light yellowish color deposits, and nitric acid immersion results in brownish deposits. Visual inspection also shows that the AAB portion of the PC+AAB mixes remains intact on the surface, whereas the PC component undergoes complete disintegration.

(a) PAM (b) PAH

(c) PAV

Fig. 9 Cubes after 28-day immersion in 10% v/v sulfuric acid solution

In the case of PAH and PAV mixing, the interface between the PC and AAB portion proves to be the weakest against acid attack, resulting in separation between the PC and AAB layers, as shown in Fig. 9. As concrete specimens are alkaline in nature, the acids react with concrete resulting in the formation of salts that are deposited. Sulfuric acid immersion is found to cause the maximum deterioration of the specimens by visual inspection. Fig. 9 shows the effect of sulfuric acid immersion on the PAM, PAH, and PAV concrete specimens. Compressive strength test results show that the residual strength is least in the case of sulfuric acid immersion.

Figs. 10-11 show the deterioration of PC+AAB paste samples after immersion in acid. Similar to concrete specimens, paste samples immersed in sulfuric acid suffered greater deterioration, followed by nitric acid and hydrochloric acid. It is evident from Figs. 10 and 11 that paste samples with greater fly ash content (FS 0 and FS 30) experienced considerable damage with samples not

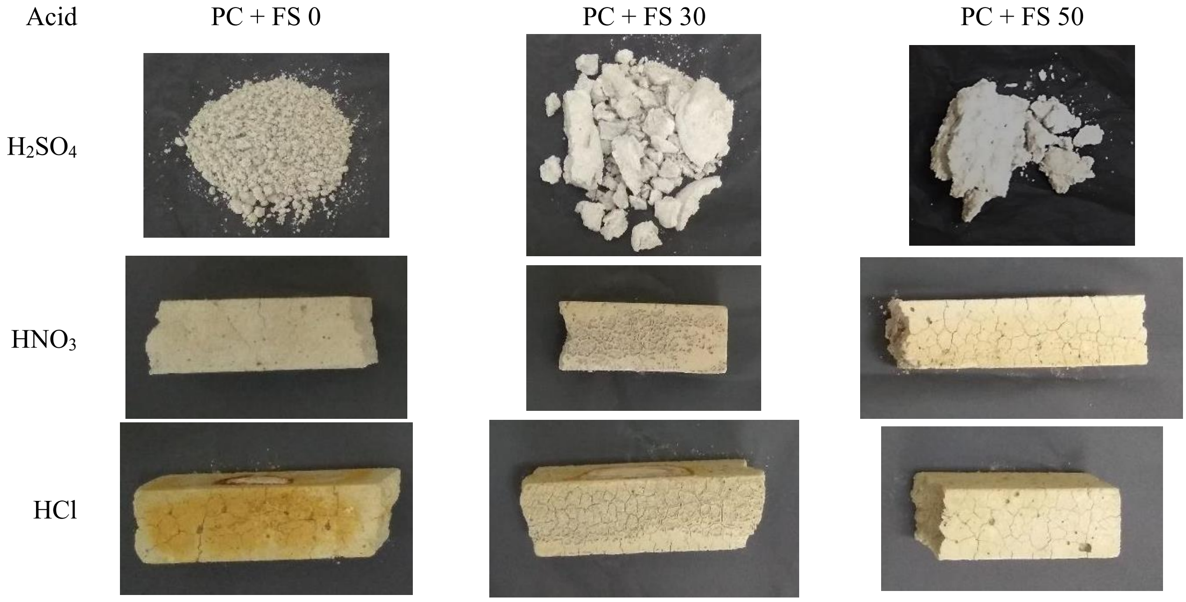

Fig. 10 PC+AAB paste specimens after drying in an oven

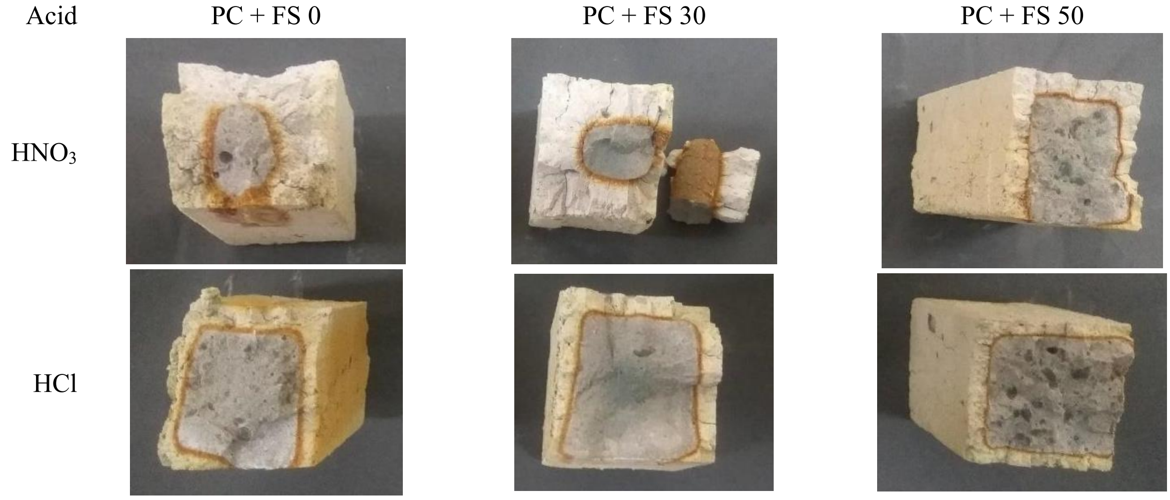

Fig. 11 Unaffected central core of PC+AAB paste specimens after immersion in acid

retaining their shape after immersion for 28 days. Though FS 50 samples subjected to sulfuric acid immersion experienced significant damage, it retained the shape to a greater extent in comparison to FS 0 and FS 30. Enhanced resistance to acid attack with increasing slag content is attributed to pore refinement and further improved durability. Fig. 11 shows the corrosion depth on immersion in acid solutions, qualitatively.

Since the samples were completely disintegrated on immersion in sulfuric acid, the samples immersed in nitric acid and hydrochloric acid are presented in Fig. 11. The unaffected central core is distinct from Fig. 11. Nitric acid has a substantial degrading effect on the PC+AAB mixes compared to hydrochloric acid.

Corrosion is visibly higher in FS 0 and FS 30 samples on immersion in nitric acid, whereas all the three mixes, FS 0, FS 30, and FS 50, show comparable corrosion on immersion in hydrochloric acid. Visual assessment of both concrete and paste samples provided a clear insight into the extent of deterioration on immersion in acid solutions.

4.2.2 Compressive strength test

The results for the mean compressive strength of triplicate specimens for each mix proportion are provided in Table 8 along with the corresponding coefficients of variation (COV%), within square brackets as [mean strength, COV%]. The percentage of strength retained after acid immersion in each case is provided within parentheses along with the compressive strength values.

Compressive strength values increase as the slag content in the AAB mixtures increase. This is mainly because the slag particles are much finer than the normal PC and fly ash particles, which results in the particles being able to easily fill up the voids in the matrix, which later, on hardening, results in a rise in the strength. It is evident that as the immersion medium changes from sulfuric acid to nitric acid, i.e., a strong acid to medium acid, the reduction in compressive strength of the specimens is lesser. This is

Table 8 Compressive strength testing results for different exposure conditions

Mixture	AAB Composition	Exposure Conditions			
		Air	HCl	H_2SO_4	HNO_3
100% PC (no replacement)	-	[58.79, 0.88]	[16.25, 2.40] (27.64%)	[7.96, 5.55] (13.5%)	[25.01, 1.64] (42.54%)
PAH	50% PC + 50% FS 0	[36.64, 4.78]	[15.13, 8.69] (41.75%)	[13.22, 11.27] (36.08%)	[20.47, 6.76] (55.86%)
	50% PC + 50% FS 30	[39.83, 3.38]	[22.30, 4.53] (55.98%)	[15.53, 7.37] (38.99%)	[26.53, 4.01] (66.60%)
	50% PC + 50% FS 50	[42.46, 8.86]	[19.67, 14.34] (46.32%)	[16.33, 19.58] (38.45%)	[26.53, 11.20] (62.48%)
PAV	50% PC + 50% FS 0	[22.70, 7.41]	[14.73, 8.56] (64.88%)	[11.71, 12.21] (51.58%)	[17.76, 7.48] (78.23%)
	50% PC + 50% FS 30	[27.24, 4.74]	[15.53, 6.24] (57.01%)	[14.73, 7.46] (54.07%)	[22.70, 4.50] (83.33%)
	50% PC + 50% FS 50	[28.84, 12.52]	[19.67, 13.76] (68.20%)	[14.34, 21.40] (49.72%)	[25.01, 11.40] (86.71%)
PAM	50% PC + 50% FS 0	[31.86, 5.56]	[13.62, 9.75] (42.74%)	[10.59, 14.21] (33.23%)	[15.13, 9.24] (47.48%)
	50% PC + 50% FS 30	[35.05, 3.88]	[15.53, 6.57] (44.30%)	[12.10, 9.55] (34.52%)	[17.76, 6.05] (50.67%)
	50% PC + 50% FS 50	[48.5, 7.84]	[24.3, 11.73] (50.10%)	[18, 17.94] (37.11%)	[24.7, 12.15] (50.92%)

attributed to a decrease in the number of alkaline bonds in the hydrated cementitious matrix being broken. The PC+AAB specimens show greater compressive strength compared to the 100% PC specimens. The long-chain Si-O-Al polymeric bonds in the AAB matrix provide greater resistance to acid attack, as compared to the C-S-H bonds in the hydrated PC matrix. Also, the introduction of slag to the AAB specimens helps with an increase in strength due to the formation of secondary C-S-H bonds.

Compressive strength values increase as the slag content in the AAB mixtures increase. This is mainly because the slag particles are much finer than the normal PC and fly ash particles, which results in the particles being able to easily fill up the voids in the matrix, which later, on hardening, results in a rise in the strength. It is evident that as the immersion medium changes from sulfuric acid to nitric acid, i.e., a strong acid to medium acid, the reduction in compressive strength of the specimens is lesser. This is attributed to a decrease in the number of alkaline bonds in the hydrated cementitious matrix being broken. The PC+AAB specimens show greater compressive strength compared to the 100% PC specimens.

The long-chain Si-O-Al polymeric bonds in the AAB matrix provide greater resistance to acid attack, as compared to the C-S-H bonds in the hydrated PC matrix. Also, the introduction of slag to the AAB specimens helps with an increase in strength due to the formation of secondary C-S-H bonds.

The lower strength retention of FS 0 in all the cases and FS 50 in the majority of the tested cases is attributed to the fact that as we move from FS 0 specimens to FS 50 specimens, there are secondary C-S-H bonds in addition to the polymeric bonds resulting from alkali activation of fly ash. These C-S-H bonds provide a greater number of sites for the acids to attack, leading to uncertainties in the microstructure of the concrete. This is also the reason for the COV% of greater than 10 for the PC+FS 50 specimens when exposed to different acids. However, the strength retention of these mixes is still greater than those of the 100% PC mixes. Hence, the replacement of the PC by AAB is clearly advantageous. The recommended technique for partial replacement of PC with AAB, especially on exposure to acid attack is governed by the strength as well as deterioration of the integrity of the concrete matrix. Hence, corrosion depth analyses are presented below to supplement the findings from this section.

Table 9 Corrosion depth results for different exposure conditions

Mixture	Corrosion Depth (mm)
100% PC (no replacement)	8
50% PC + 50% FS 0	6
50% PC + 50% FS 30	4
50% PC + 50% FS 50	4

4.2.3 Test for corrosion depth

Corrosion depth is measured for the 100% PC concrete specimens and for the PAM combination mixes. Corrosion depth measurement for PAH and PAV mixes become redundant as the PC and AAB portions separate out at the interface. Visual inspection of the PAH and PAV specimens after acid immersion show that the PC layer gets deteriorated beyond serviceability within a week, whereas the AAB layer remains visually unaltered during the 28 days even though the internal microstructure undergoes deterioration. A measure of this degree of deterioration is the corrosion depth. The results are present in Table 9.

Based on the findings from strength and corrosion depth testing, the recommendations for mixing technique are presented below.

4.2.4 Recommended mixing technique

The PAH and PAV specimens show greater compressive strength than the PAM specimens on exposure to air as well as those exposed to acid solutions. The reason behind this is the dissipation of stresses through the several PC-AAB binder-interfaces that deteriorated simultaneously. For the PAH specimens, the face along the direction of casting is kept perpendicular to the direction of application of the load resulting in the two layers being in parallel, which in turn results in the symmetric distribution of stress. In the case of the PAV specimens, the load is distributed through the PC layer at the top, and the AAB layer at the bottom and vice versa, and similar results are obtained. Among the different AAB combinations, FS 30 shows the maximum percentage strength retained for the majority of the tested cases in the present study. 50% PC+50% FS 30 always exhibited higher strength retention when the mixing technique adopted is PAH.

However, there is no deducible trend observed in the results of 50% PC+50% FS 30 and 50% PC+50% FS 50 when PAV and PAM mixing techniques were used. For a few cases, 50% PC+50% FS 50 exhibited higher percentage of strength retained in the range of 0.25 to 11.2 % compared to 50% PC+50% FS 30.

The mode of mixing can depend on the strength requirement and the availability of skilled personnel. Based on all the observations, a mix proportion of 50% PC+50% FS 30 prepared with either PAH or PAV mixing technique is suggested for practical implementation under ambient conditions when there is no chance of acid attack. In case of exposure to acid attack, two possible mixing techniques can be adopted. 50% PC+50% FS 30 with PAM mixing technique can prevent complete disintegration in the case of an acid attack on all exposed concrete surfaces. However, if the acid attack is imminent on selected surfaces, then only the surfaces of the concrete element in contact with acid can be constructed from AAB; the remaining unexposed surfaces can be composed of traditional PC concrete. Depending on the direction of the acid attack, PAV or PAH mixing modes can be adopted. So, the type of mix applicable to a particular case depends on the requirements at the site and the corresponding judgement of the site personnel.

5. Conclusions

Based on the above study, the following conclusions are made:

1. PC specimens placed in an acidic environment undergo deterioration at a considerably greater rate as compared to PC+AAB mixes.
2. XRD studies show the dissolution of crystalline reaction products. Severe deterioration of the PC+AAB mix exposed to sulfuric acid is corroborated by the formation of Ca-rich phases.
3. FTIR studies reveal the formation of amorphous salt as a result of the reaction between a strong acid and the alkaline PC+AAB mixes.
4. SEM-EDS analysis provides both qualitative and quantitative degradation of samples. SEM micrographs of samples after H_2SO_4 attack show precipitation of gypsum crystals, whereas samples on exposure to HNO_3 and HCl solutions show lower morphology changes.
5. The unaffected central core of the samples corroborates with the findings from microstructural analysis and give an essence of the extent of damage on the specimen-level scale.
6. The introduction of slag to the PC+AAB mixes increases the compressive strength in all the PC+AAB mixes.
7. Among the different AAB combinations, FS 30 shows the maximum percentage strength retained for majority of the acid attacks. Hence, this mix is recommended for practical implementation.
8. The strength retention in 100% PC mixes is the least among all the mixes.
9. Corrosion depth is found to be the greatest in the case of 100% PC mixes.
10. 50% PC+50% FS 30 prepared with either PAH or PAV mixing technique is suggested for practical implementation under ambient conditions (31°C±2°C; 70% RH) when there is no chance of acid attack.
11. In case of exposure to acid attack, 50% PC+50% FS 30 with PAM mixing technique can prevent complete disintegration in the case of an acid attack on all exposed concrete surfaces.

The recommendations made in this study are based on the findings determined under the climatic conditions available in the Indian subcontinent. This study can be extended to demonstrate the effect of other climates and also the utility of 100% AAB mixes for widespread concrete construction in the future.

Acknowledgments

The authors gratefully acknowledge the technical support for performing microstructural analysis from Central Analytical Laboratory at BITS Pilani-Hyderabad Campus.

References

ACI Committee 211 (Reapproved 2009), Standard Practice for Selecting Proportions for Normal, Heavyweight, and Mass Concrete (ACI 211.1-91), American Concrete Institute.

Aiken, T.A., Kwasny, J., Sha, W. and Soutsos, M.N. (2018), “Effect of slag content and activator dosage on the resistance of fly ash geopolymer binders to sulfuric acid attack”, *Cement Concrete Res.*, **111**, 23-40. https://doi.org/10.1016/j.cemconres.2018.06.011.

Allahverdi, A. and Škvára, F. (2005), “Sulfuric acid attack on hardened paste of geopolymer cements. Part 1. Mechanism of corrosion at relatively high concentrations”, *Ceram.-Silik.*, **49**(4), 225-229.

Allahverdi, A. and Skvara, F. (2006), “Sulfuric acid attack on hardened paste of geopolymer cements-part 2. Corrosion mechanism at mild and relatively low concentrations”, *Ceram.-Silik.*, **50**(1), 1-4.

Askarian, M., Tao, Z., Adam, G. and Samali, B. (2018), “Mechanical properties of ambient cured one-part hybrid OPC-geopolymer concrete”, *Constr. Build. Mater.*, **186**, 330-337. https://doi.org/10.1016/j.conbuildmat.2018.07.160.

ASTM C311/C311M (2018), Standard Test Methods for Sampling and Testing Fly Ash or Natural Pozzolans for Use in Portland-Cement Concrete, ASTM International, West Conshohocken, PA.

ASTM C33/C33M (2017), Standard Specification for Concrete Aggregates, ASTM International, West Conshohocken, PA.

ASTM C39/C39M (2013), Standard Test Method for Compressive Strength of Cylindrical Concrete Specimens, ASTM International, West Conshohocken, PA.

ASTM C494 (2013), Specification for Chemical Admixtures for Concrete, ASTM International, West Conshohocken, PA.

ASTM C618 (2013), Standard Specification for Coal Fly Ash and Raw or Calcined Natural Pozzolan for Use in Concrete, ASTM International, West Conshohocken, PA.

ASTM C989 (2013), Standard Specification for Slag Cement for Use in Concrete and Mortars, ASTM International, West Conshohocken, PA.

Bakharev, T., Sanjayan, J.G. and Cheng, Y.B. (2003), "Resistance of alkali-activated slag concrete to acid attack", *Cement Concrete Res.*, **33**(10), 1607-1611. https://doi.org/10.1016/S0008-8846(03)00125-X.

Bernal, S.A., Rodríguez, E.D., Mejía de Gutiérrez, R. and Provis, J.L. (2012), "Performance of alkali-activated slag mortars exposed to acids", *J. Sustain. Cement Bas. Mater.*, **1**(3), 138-151. https://doi.org/10.1080/21650373.2012.747235.

Central Electricity Authority (CEA) (2017), Report on Fly Ash Generation at Coal/lignite Based Thermal Power Stations and its Utilization in the Country for The Year 2016-17, New Delhi.

Dassekpo, J.B.M., Zha, X., Zhan, J. and Ning, J. (2017), "The effects of the sequential addition of synthesis parameters on the performance of alkali activated fly ash mortar", *Resul. Phys.*, **7**, 1506-1512. https://doi.org/10.1016/j.rinp.2017.04.019.

De Ceukelaire, L. (1992), "The effects of hydrochloric acid on mortar", *Cement Concrete Res.*, **22**(5), 903-914. https://doi.org/10.1016/0008-8846(92)90114-B.

Diaz-Loya, E.I., Allouche, E. and Vaidya, S. (2011), "Mechanical properties of fly-ash-based geopolymer concrete", *ACI Mater. J.*, **108**(3), 300-306.

Ding, Y., Dai, J.G. and Shi, C.J. (2016), "Mechanical properties of alkali-activated concrete: A state-of-the-art review", *Constr. Build. Mater.*, **127**, 68-79. https://doi.org/10.1016/j.conbuildmat.2016.09.121.

Duxson, P. (2009), "Geopolymer precursor design", *Geopolymers: Structure, Processing, Properties and Industrial Applications*, Eds. Provis, J.L. and van Deventer, J.S.J., Boca Raton, Florida.

Fang, G., Ho, W.K., Tu, W. and Zhang, M. (2018), "Workability and mechanical properties of alkali-activated fly ash-slag concrete cured at ambient temperature", *Constr. Build. Mater.*, **172**, 476-487. https://doi.org/10.1016/j.conbuildmat.2018.04.008.

Gomez, J.C., Calvet, N., Starace, A.K. and Glatzmaier, G.C. (2013), "Ca $(NO_3)_2$-$NaNO_3$-KNO_3 molten salt mixtures for direct thermal energy storage systems in parabolic trough plants", *J. Sol. Energy Eng.*, **135**(2), 021016. https://doi.org/10.1115/1.4023182.

Gu, L., Visintin, P. and Bennett, T. (2018), "Evaluation of accelerated degradation test methods for cementitious composites subject to sulfuric acid attack; application to conventional and alkali-activated concretes", *Cement Concrete Compos.*, **87**, 187-204. https://doi.org/10.1016/j.cemconcomp.2017.12.015.

Hardjito, D. and Rangan, B.V. (2005), "Development and properties of low-calcium fly ash-based geopolymer concrete", Curtin University of Technology Research Report GC1, Curtin University, Perth, Australia.

IS 516-1959 (2018), Methods of Tests for Strength of Concrete, Bureau of Indian Standards, New Delhi, India.

Ismail, I., Bernal, S.A., Provis, J.L., San Nicolas, R., Hamdan, S. and van Deventer, J.S. (2014), "Modification of phase evolution in alkali-activated blast furnace slag by the incorporation of fly ash", *Cement Concrete Compos.*, **45**, 125-135. https://doi.org/10.1016/j.cemconcomp.2013.09.006.

Junaid, M.T. (2017), "Properties of ambient cured blended alkali activated cement concrete", *IOP Conf. Ser.: Mater. Sci. Eng.*, **264**(1), 012004.

Junaid, M.T., Kayali, O., Khennane, A. and Black, J. (2015), "A mix design procedure for low calcium alkali activated fly ash-based concretes", *Constr. Build. Mater.*, **79**, 301-310. https://doi.org/10.1016/j.conbuildmat.2015.01.048.

Kani, E.N., Allahverdi, A. and Provis, J.L. (2018), "Calorimetric study of geopolymer binders based on natural pozzolan", *J. Therm. Anal. Calorim.*, **127**(3), 2181-2190. https://doi.org/10.1007/s10973-016-5850-7.

Kar, A. (2013) "Characterizations of concretes with alkali-activated binder and correlating their properties from micro-to specimen level", PhD Thesis, West Virginia University, Morgantown, West Virginia.

Kar, A., Ray, I., Unnikrishnan, A. and Halabe, U. B. (2016), "Prediction models for compressive strength of concrete with alkali-activated binders", *Comput. Concrete*, **17**(4), 523-539. http://dx.doi.org/10.12989/cac.2016.17.4.523.

Ko, L.S., Beleña, I., Duxson, P., Kavalerova, E., Krivenko, P.V., Ordoñez, L.M., Tagnit-Hamou, A. and Winnefeld, F. (2014), "AAM concretes: standards for mix design/formulation and early-age properties", *Alkali Activated Materials: State-of-the-Art Report, RILEM TC 224-AAM*, Eds. Provis, J.L. and van Deventer, J.S.J., Springer, Dordrecht, Netherlands.

Kumar, S., Kumar, R. and Mehrotra, S.P. (2010), "Influence of granulated blast furnace slag on the reaction, structure and properties of fly ash based geopolymer", *J. Mater. Sci.*, **45**(3), 607-615. https://doi.org/10.1007/s10853-009-3934-5.

Lee, N.K. and Lee, H.K. (2016), "Influence of the slag content on the chloride and sulfuric acid resistances of alkali-activated fly ash/slag paste", *Cement Concrete Compos.*, **72**, 168-179. https://doi.org/10.1016/j.cemconcomp.2016.06.004.

Lloyd, R.R., Provis, J.L. and van Deventer, J.S.J. (2012), "Acid resistance of inorganic polymer binders. 1. Corrosion rate", *Mater. Struct.*, **45**(1-2), 1-14. https://doi.org/10.1617/s11527-011-9744-7.

Luukkonen, T., Abdollahnejad, Z., Yliniemi, J., Kinnunen, P. and Illikainen, M. (2018), "One-part alkali-activated materials: a review", *Cement Concrete Res.*, **103**, 21-34. https://doi.org/10.1016/j.cemconres.2017.10.001.

Madavarapu, S.B. (2014), "FTIR analysis of alkali activated slag and fly ash using deconvolution techniques", M.S. Thesis, Arizona State University, Tempe, AZ.

Mazhar, S. and GuhaRay, A. (2020), "Stabilization of expansive clay by fibre-reinforced alkali-activated binder: an experimental investigation and prediction modelling", *Int. J. Geotech. Eng.*, 1-17. doi.org/10.1080/19386362.2020.1775358.

Monteny, J., Vinke, E., Beeldens, A., DeBelie, N., Taerwe, L., Van Gemert, D. and Verstraete, W. (2000), "Chemical, microbiological, and in situ methods for biogenic sulfuric acid corrosion of concrete", *Cement Concrete Res.*, **304**, 623-634. https://doi.org/10.1016/S0008-8846(00)00219-2.

Nath, P. and Sarker, P.K. (2014), "Effect of GGBFS on setting, workability and early strength properties of fly ash geopolymer concrete cured in ambient condition", *Constr. Build. Mater.*, **66**, 163-171. https://doi.org/10.1016/j.conbuildmat.2014.05.080.

Oelkers, E.H. and Schott, J. (1995), "Experimental study of anorthite dissolution and the relative mechanism of feldspar hydrolysis", *Geochim. Cosmochim. Acta*, **59**(24), 5039-5053. https://doi.org/10.1016/0016-7037(95)00326-6.

Pacheco-Torgal, F., Gomes, J. and Jalali, S. (2010), "Durability and environmental performance of alkali-activated tungsten mine waste mud mortars", *J. Mater. Civil Eng.*, **22**(9), 897-904.

https://doi.org/10.1061/(ASCE)MT.1943-5533.0000092.

Palacios, M. and Puertas, F. (2011), "Effectiveness of mixing time on hardened properties of water glass activated slag pastes and mortars", *ACI Mater. J.*, **108**(1), 73-78.

Pavlík, V. (1994), "Corrosion of hardened cement paste by acetic and nitric acids part II: formation and chemical composition of the corrosion products layer", *Cement Concrete Res.*, **24**(8), 1495-1508. https://doi.org/10.1016/0008-8846(94)90164-3.

Provis, J.L. and van Deventer, J.S.J. (2014), Alkali Activated Materials: State-of-the-Art Report, RILEM TC 224-AAM, Springer, Dordrecht,.

Provis, J.L., Bílek, V., Buchwald, A., Dombrowski-Daube, K. and Varela, B. (2014) "Durability and testing - physical processes", Alkali Activated Materials: State-of-the-Art Report, RILEM TC 224-AAM, Eds. Provis, J.L. and van Deventer J. S. J., Springer, Dordrecht, Netherlands.

Provis, J.L., Palomo, A. and Shi, C. (2015), "Advances in understanding alkali-activated materials", *Cement Concrete Res.*, **78**, 110-125. https://doi.org/10.1016/j.cemconres.2015.04.013.

Ramagiri, K.K. and Kar, A. (2019), "Effect of precursor combination and elevated temperatures on the microstructure of alkali-activated binder", *ICJ*, **93**(10), 34-43. https://doi.org/10.1016/j.matpr.2020.01.093.

Ramagiri, K.K., Chauhan, D., Gupta, S., Kar, A. and Adak, D. (2020), "Evaluation of structural performance of concrete with ambient-cured alkali-activated binders", *Proceedings of SECON'19, SECON 2019*, Lecture Notes in Civil Engineering, Springer, **46**, May.

Rangan, B. (2010), "Design and manufacture of fly-ash based geopolymer concrete", *Concr. Aust.*, **34**(2), 37-43.

Rangan, B.V. (2008), "Low-calcium fly-ash-based geopolymer concrete", *Concrete Construction Engineering Handbook*, Ed. Nawy, E.G., CRC Press, New York.

Rashad, A.M. (2013), "Properties of alkali-activated fly ash concrete blended with slag", *Iran. J. Mater. Sci. Eng.*, **10**(1), 57-64.

Shekhovtsova, J., Kovtun, M. and Kearsley, E.P. (2015), "Evaluation of short-and long-term properties of heat-cured alkali-activated fly ash concrete", *Mag. Concrete Res.*, **67**(16), 897-905. https://doi.org/10.1680/macr.14.00377.

Shi, C. (2003), "Corrosion resistance of alkali-activated slag cement", *Adv. Cement Res.*, **15**(2), 77-81. https://doi.org/10.1680/adcr.2003.15.2.77.

Shi, C. and Stegmann, J.A. (2000), "Acid corrosion resistance of different cementing materials", *Cement Concrete Res.*, **30**(5), 803-808. https://doi.org/10.1016/S0008-8846(00)00234-9.

Song, X., Marosszeky, M., Brungs, M. and Munn, R. (2005), "Durability of fly ash based geopolymer concrete against sulphuric acid attack", *10th International Conference on the Durability of Building Materials and Components*, Lyon, France.

Temuujin, J., Minjigmaa, A., Lee, M., Chen-Tan, N. and Van Riessen, A. (2011), "Characterisation of class F fly ash geopolymer pastes immersed in acid and alkaline solutions", *Cement Concrete Compos.*, **33**(10), 1086-1091. https://doi.org/10.1016/j.cemconcomp.2011.08.008.

Wallah, S.E. and Rangan. B.V. (2006), "Low-calcium fly ash-based geopolymer concrete: long-term properties", Curtin University of Technology, Perth, Australia.

Xie, J., Wang, J., Rao, R., Wang, C. and Fang, C. (2019), "Effects of combined usage of GGBS and fly ash on workability and mechanical properties of alkali activated geopolymer concrete with recycled aggregate", *Compos. Part B: Eng.*, **164**, 179-190. https://doi.org/10.1016/j.compositesb.2018.11.067.

Ye, H. and Huang, L. (2020)", Degradation mechanisms of alkali-activated binders in sulfuric acid: The role of calcium and aluminum availability", *Constr. Build. Mater.*, **246**, 118477. https://doi.org/10.1016/j.conbuildmat.2020.118477.

Yip, C., Lukey, G.C., Provis, J.L. and van Deventer, J.S.J. (2008), "Effect of calcium silicate sources on geopolymerization", *Cement Concrete Res.*, **38**(4), 554-564. https://doi.org/10.1016/j.cemconres.2007.11.001.

Yip, C.K., Lukey, G.C. and Van Deventer, J.S. (2005), "The coexistence of geopolymeric gel and calcium silicate hydrate at the early stage of alkaline activation", *Cement Concrete Res.*, **35**(9), 1688-1697. https://doi.org/10.1016/j.cemconres.2004.10.042.

Zhang, W., Yao, X., Yang, T. and Zhang, Z. (2018), "The degradation mechanisms of alkali-activated fly ash/slag blend cements exposed to sulphuric acid", *Constr. Build. Mater.*, **186**, 1177-1187. https://doi.org/10.1016/j.conbuildmat.2018.08.050.

Zhao, M., Zhang, X. and Zhang, Y.J. (2011), "Resistance of hydrated cement paste to acid attack and kinetics analysis of corrosion", *Adv. Mater. Res.*, **163**, 3133-3137. https://doi.org/10.4028/www.scientific.net/AMR.163-167.3133.

CC